inorganics

MDPI

Article

Employing Molecular Dynamics Simulations to Explore the Behavior of Diphenylalanine Dipeptides in Graphene-Based Nanocomposite Systems

Elena Markopoulou [1], Panagiotis Nikolakis [2], Gregory Savvakis [3] and Anastassia N. Rissanou [4,*]

[1] Department of Materials Science and Engineering, University of Crete, 71409 Heraklion, Greece; mst1621@edu.materials.uoc.gr
[2] Department of Physics, School of Science, National and Kapodistrian University of Athens, 15784 Athens, Greece; sph2000124@uoa.gr
[3] Physics Department, University of Ioannina, 45110 Ioannina, Greece; pph400885@uoi.gr
[4] Theoretical & Physical Chemistry Institute, National Hellenic Research Foundation, 48 Vassileos Constantinou Avenue, 11635 Athens, Greece
* Correspondence: trissanou@eie.gr

Abstract: Utilizing all-atom molecular dynamics simulations, in the current study, we examine how three different graphene-based nanosheets (pristine graphene, graphene oxide and edge-functionalized graphene) impact the self-assembly mechanism of diphenylalanine dipeptides in aqueous solutions. By comparing the conformational properties and dynamics of diphenylalanine dipeptides in the presence of each nanosheet, we elucidate the effects of the existence of functional groups, their type, and their position on the formed nanostructures. We quantify the interaction energy between diphenylalanine dipeptides and the nanosheets, analyzing various energetic components, to gain insights into the driving forces for the assembly procedure in the nanocomposite systems. Dipeptides readily coat nanosheets due to their high surface affinity. Subsequent diphenylalanine self-assembly is determined by the nanofiller type: in the systems with graphene oxide and edge functionalized graphene, there is an increase of the interfacial layer thickness, while in the system with pristine graphene a structure extended on top of the coating layer is formed. Additionally, we monitor how dipeptides facilitate the dispersion of graphene-based nanosheets in aqueous solution. The findings of this work enhance our understanding of the interplay between diphenylalanine dipeptides and graphene-based nanosheets, paving the way for the rational design of novel materials with tailored properties for specific applications.

Keywords: diphenylalanine dipeptides; graphene-based nanosheets; molecular dynamics; nanostructures; self-assembly

check for updates

Academic Editors: Ben McLean and Alister Page

Received: 4 February 2025
Revised: 10 March 2025
Accepted: 14 March 2025
Published: 19 March 2025

Citation: Markopoulou, E.; Nikolakis, P.; Savvakis, G.; Rissanou, A.N. Employing Molecular Dynamics Simulations to Explore the Behavior of Diphenylalanine Dipeptides in Graphene-Based Nanocomposite Systems. *Inorganics* **2025**, *13*, 92. https://doi.org/10.3390/inorganics13030092

Copyright: © 2025 by the authors. Licensee MDPI, Basel, Switzerland. This article is an open access article distributed under the terms and conditions of the Creative Commons Attribution (CC BY) license (https://creativecommons.org/licenses/by/4.0/).

1. Introduction

Since its discovery, graphene has been extensively studied due to its unique properties that include remarkable mechanical strength, supreme thermal conductivity, and high electronic conductivity [1–3]. The latter makes this material the best conductor of electricity known thus far. For this reason, the majority of its applications are in the field of electronics [3–7]. However, graphene can also be implemented in biomedicine in a plethora of ways, such as, in the manufacturing of thinner and lighter biosensors with increased sensitivity in detecting biological fluids or diseases [8], or in tissue engineering [9–11]. Another emerging use of graphene is as a substrate for studying structural changes in biomolecules [12–16].

The main roadblocks in the fabrication of graphene nanocomposites are the lack of functional groups at the surface of pristine graphene that could facilitate the anchoring of biomolecules, as well as the poor dispersion capabilities of pristine graphene in water and most organic solvents due to its high solvo-phobicity [17–19]. Consequently, graphene derivates are used instead, with the main one being graphene oxide (GO), which occurs with chemical processing of pristine graphene. Graphene oxide has increased solubility in aqueous solutions thanks to its functional groups that include epoxides, hydroxyls, and carboxylic acids [3,20]. Other types of functionalized graphene are also used, such as the edge-functionalized graphene with functional groups only around its edges [21,22].

The primary concern in implementing graphene in bionanotechnology is the molecule's toxic effects after insertion in the human body, which are related to its physicochemical properties. According to previous studies, researchers try to minimize graphene's biotoxicity by downscaling the size of the graphitic surfaces and/or functionalizing them with biomolecules, forming nanomaterials for biomedical applications [23–25].

Biomolecules such as proteins and peptides are widely incorporated in nanotechnology due to their wide range of functionalities [26,27]. Peptide self-assembly in particular, despite not being a well understood process, has contributed greatly to the design of highly specialized drug delivery systems that exhibit controlled drug release [26], low immunogenicity, and specific recognition ability [28–30]. In recent years, the interactions between biomolecules and surfaces have been more intensively studied in an effort to better understand their association [31] as well as to identify their key recognition motifs [32].

An increasing number of novel nanomaterials are implemented in medicine for the prevention and treatment of a plethora of diseases, such as Alzheimer's disease (AD) [33,34]. Although the mechanism of AD pathogenesis is not fully understood, the amyloid plaque hypothesis is widely accepted as the primary cause. Aβ, a hydrophobic peptide consisting of 39–42 amino acids, is the main component of amyloid aggregates and is derived from the cleavage of b-amyloid precursor protein (APP). Aβ undergoes secondary structural transitions and misfolds, forming oligomers that aggregate into fibrils. This process can induce reactive oxygen species (ROS), oxidation, and cellular damage [33]. The accumulation of abnormally folded Aβ peptides on neural cells is arguably the most critical step of this mechanism, as Aβ oligomers and fibrils induce neurotoxicity resulting in metabolic malfunction and neuronal cell death. Consequently, preventing Aβ fibrillation, disassembling mature aggregates, and facilitating Aβ elimination are essential for the prevention and treatment of Alzheimer's disease [33,35].

One of the nanomaterials implemented to achieve this is graphene and its derivatives, taking advantage of the natural tendency of amyloid fibrils to adhere to both hydrophobic and hydrophilic surfaces [36]. Previous molecular dynamics simulations studies by Yang et al. focused on the influence of graphene on the degradation of amyloid fibrils and demonstrated that graphene nanosheets can proficiently interfere with the architecture of amyloid fibrils by embedding themselves within the fibrils. This results in structural distortion, separation into smaller fragments, and the extraction of individual peptides through robust dispersion interactions enabled by graphene's extensive surface area and π-π* stacking interactions with the aromatic residues of the extracted amyloid peptides [35,37]. These results indicate that the disruption of Aβ fibril structures is possible due to the stronger interaction of Aβ peptides with graphene than with the pre-formed fibril structure. Additionally, they demonstrated that graphene oxide effectively delays and diminishes the aggregation of Aβ monomers into fibrils through Thioflavin-T fluorescence assays and used atomic force microscopy (AMF) to prove a correlation between GO concentration and fibril formation or disassembly efficiency [35,38,39]. The size effects of GO nanosheets on Aβ peptide aggregation have been studied experimentally by Wang et al. using quartz crys-

tal microbalance (QCM), circular dichroism (CD) spectroscopy, and AFM measurements, concluding that larger GO surfaces present a stronger modulation effect on the aggregation of amyloid peptides opening new pathways in controlling the self-assembly of amyloid peptide nanostructures [40]. In addition, replica exchange molecular dynamics simulations were used and further validated that the larger contact surface area of GO better inhibits Aβ oligomerization by weakening interpeptide interactions [41,42]. Furthermore, He et al. examined the thermodynamics and kinetics of Aβ fibril elongation on GO surfaces with various oxidative degrees, using a combination of experimental and computational methods, and revealed that low oxidative GO promotes fibril elongation, while high oxidative GO inhibits fibril elongation [43].

The large and complex structure of proteins often limits the downscaling and controlled fabrication of novel nanomaterials. For this reason, many researchers turn their attention to peptides, as their simpler structure and high biological functionality make them ideal candidates as building blocks for nanoscale materials. No et al. studied the self-assembly of various peptide sequences on pristine graphene using atomistic molecular dynamics simulations. These peptides were designed so they consist of charged hydrophilic residues that do not geometrically disturb the hydrogen bonding between β-strands and aromatic residues, which enhance the interaction between peptide and graphene. It was found that peptide self-assembly on pristine graphene results in the slight n-doping of the surface without altering its intrinsic properties [44,45]. Previous studies on the adsorption propensity of different amino acids on graphene and graphene oxide have proven that aromatic amino acids adsorb onto graphene through π-π* interactions, while positively charged amino acids exhibit stronger affinity to graphene oxide through electrostatic interactions [20]. Moreover, Camden N.A. et al. demonstrated that arginine, glutamine, and asparagine are the amino acids with the strongest affinity to pristine graphene by calculating the binding enthalpies of GXG tripeptides, with X being each of the twenty amino acids naturally found in the human body, using classical molecular dynamics simulations [46]. Other characteristics to consider when fabricating peptide-graphene composite materials, besides binding enthalpy, are solvent effects and the physicochemical properties of the peptide aggregates, as they could potentially determine the functionality of the final material [47,48].

A peptide that has gained great popularity is diphenylalanine (FF) due to its ability to form various structures as a result of its self-assembly propensity. The shape of the aggregate formed by FF dipeptides in solution depends heavily on the nature of the solvent, the solution's concentration, environmental conditions, such as temperature and pressure, and the possible presence of other solutes. When dispersed in water under ambient conditions, FF dipeptides tend to self-assemble into well-defined fibers and/or tubes [49–51]. Extensive theoretical and experimental studies have concluded that hydrogen bonding is the major driving force of FF self-assembly, while the molecule's aromatic side chains are responsible for the formation of highly ordered structures [52–55]. FF nanotubes are proven to be very stable in water and present a plethora of remarkable properties. They have potential applications as cost-effective nontoxic scaffolds that are adjustable with biochemical processes, as templates for metal nanowires and photo-switching nanoribbons, and as scaffolds for electronic interconnects and microfluidic channels [56,57]. One important application of self-assembled FF nanostructures is their application as sensors. These sensors are used for the detection of various biomedical actions such as coughing, finger movement, and arterial pulse monitoring [58].

In an experimental study by Bhattacharya et al. [59], UV resonance Raman (UVRR) spectroscopy was effectively used to characterize the self-assembly of diphenylalanine peptides with functionalized graphene nanoplatelets and their self-assembly into nanotubes.

These structures are similar to the ones observed in aqueous solutions of FF in the absence of graphene. The immediate assembly of peptide–graphene nanotubes upon mixing FF peptides with graphene dispersions was observed by SEM. Furthermore, SEM and AFM imaging have revealed that FF forms a network of micro-and nanotubes in FF/GO nanocomposites. GO addition alters the morphology but maintains tube self-assembly [60]. A combined experimental and simulation work investigated the self-assembly of FF and YY dipeptides with GO and copper ions. The morphology and aggregation of peptide assemblies were analyzed using various spectroscopic techniques, whereas the simulation study was performed using the Density Functional Theory (DFT) framework. Results revealed that the aggregation of dipeptides was influenced by their interaction with GO. The hydrophobic dipeptide FF preferentially gathers at the edges of the GO nanosheets, while the more hydrophilic dipeptide YY tends to cover the basal planes of the nanosheets [24].

Thus far, to the best of our knowledge, the interactions between FF and graphitic surfaces have been theoretically studied using periodic pristine graphene or graphene oxide nanosheets with both DFT and molecular dynamics simulations [22,24,45,61]. It has been proven that FF's aromatic groups exhibit a relatively strong interaction with the surface through the formation of π-π^* bonds with the carbon atoms of the graphene sheet [61]. Since the aromatic rings have the same symmetry as the graphene lattice, the energetically favorable conformation of the adsorbed FF dipeptides is parallel to the surface. The adsorption energy and adsorption distance of an FF dipeptide on a periodic pristine graphene nanosheet have been calculated equal to -0.99 eV and 2.83 Å, respectively, through DFT simulations by Silva-Alves et al. [45]. The group also found that the interaction between FF aromatic rings and graphene results in a charge transfer from the adsorbed FF dipeptide to the surface [36,45]. In aqueous solutions with a higher peptide concentration, it has been proven that after the formation of FF-graphene interfaces, the spare dipeptides aggregate onto the peptide layers. The stability of such interfaces is dependent on the nature and structure of the peptides [61]. This phenomenon, however, allows for the fabrication of nanocomposite materials of various structures with modified characteristics best suited for the intended applications.

Therefore, the focus of the current study is a detailed investigation of different graphene-based nanosheets as nanofillers in corresponding nanocomposites with FF. The different effect of pristine graphene (PG), graphene oxide (GO), and edge functionalized graphene (FG) on the self-assembly mechanism of FF dipeptides in water, under ambient conditions, is examined, using all-atom molecular dynamics (MD) simulations. A comparison of the conformational properties of the FF and their dynamics in the presence of the different nanofillers is conducted, emphasizing the effect of the type and the position of the functional groups. In addition, a quantification of the interaction energy of FF with the nanosheets and a detailed calculation of the various energetic components provides information for the interplay between the self-assembly propensity of FF and the formation of FF-graphene nanostructures. Furthermore, the way in which dipeptides facilitate the dispersion of graphene-based nanosheets in aqueous solutions is also monitored.

The information revealed from this work promotes the understanding of the interplay between FF dipeptides and graphene-based nanosheets, advancing the rational design of novel materials aiming to desired applications.

2. Results and Discussion

2.1. Conformational Properties

Driven by their hydrophobic interactions, both diphenylalanine molecules and graphene flakes exhibit a strong tendency to form assemblies. A measure that quantifies the assembly propensity both between similar and dissimilar molecules is the pair

radial distribution function, g(r), (RDF). It is known that FF molecules have strong self-assembly propensity in aqueous solution resulting in nanotube formation [51,53]. However, in the presence of graphene-based flakes, there is a competition between the self-attraction and the attraction with the nanosheets, which is reflected in Figure 1.

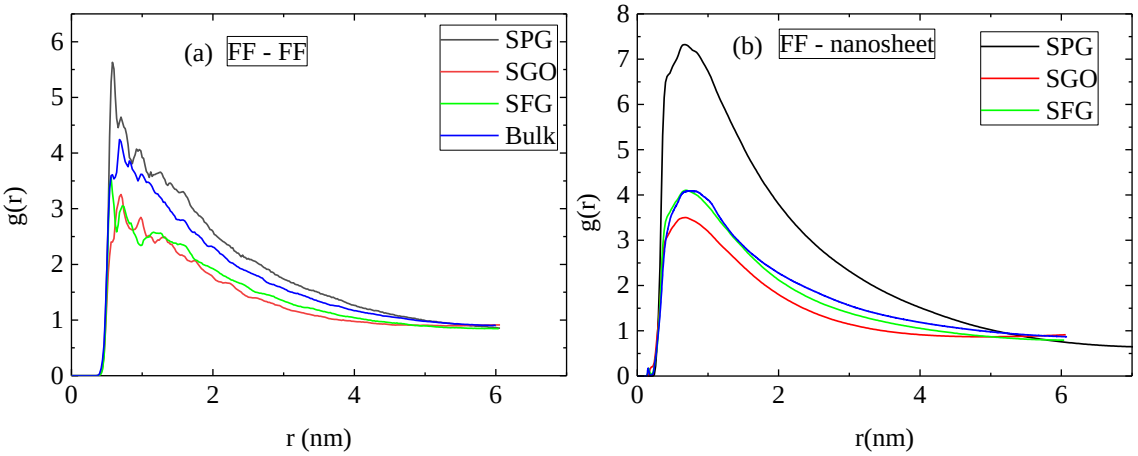

Figure 1. The pair radial distribution function, g(r), calculated (**a**) between the center of mass of FF dipeptides for SPG, SGO, and SFG systems and for a reference bulk system of 600 FF dipeptides in water and (**b**) between FF atoms and atoms of the nanosheets in SPG, SGO and SFG systems.

Figure 1a portrays the RDF between the center of mass of FF dipeptides in the three systems together with the corresponding function of FF in water (bulk system). Data have been collected from the equilibrated part of the trajectory. The comparison shows a reduction in the strength of the self-assembly in the nanocomposite systems with functionalized graphene nanofillers, whereas, for the system with pristine graphene, RDF has an almost equal height peak with that of bulk. This behavior suggests a different arrangement of dipeptides with respect to the nanofillers and, consequently, different self-assembly in the three nanocomposites. The RDF between atoms of FF dipeptides and atoms of graphene-based flakes is presented in Figure 1b. Although all three curves peak at the same distance of 1 nm, there is an obvious preference of FF for PG, FG follows with a considerably lower peak, while GO has the lowest peak. This comes as a result of the existence of functional groups, which do not allow the very close proximity of FF to the functionalized sheets.

In Figure 2a–c, the RDFs between FF and nanosheets, calculated between the atoms of the graphene-based flakes and the center of mass of FF, are compared with the FF-FF curves of Figure 1a for each system correspondingly. The higher peaks of RDFs between FF and nanosheets in all systems indicate that dipeptides exhibit a greater affinity for graphene-based surfaces than for each other. As a result, FF molecules spread along the sheets forming a layer of dipeptides on both sides of the flakes. The difference between FF-FF and FF-nanosheet RDFs is more pronounced in the SPG system, in favor of the FF-PG pair, where in addition to the higher peak height, the curve is much broader, indicating extended structures of FF on PG.

The dimensions of the individual FF molecules, as they are quantified through two measures, the radius of gyration (R_g) and the end-to-end distance of the backbone (d), are presented in Table 1. Values are identical among the systems, as well as similar to the corresponding values in bulk, thus, the dimensions of the individual dipeptides are unaffected by the existence and the type of the nanofiller.

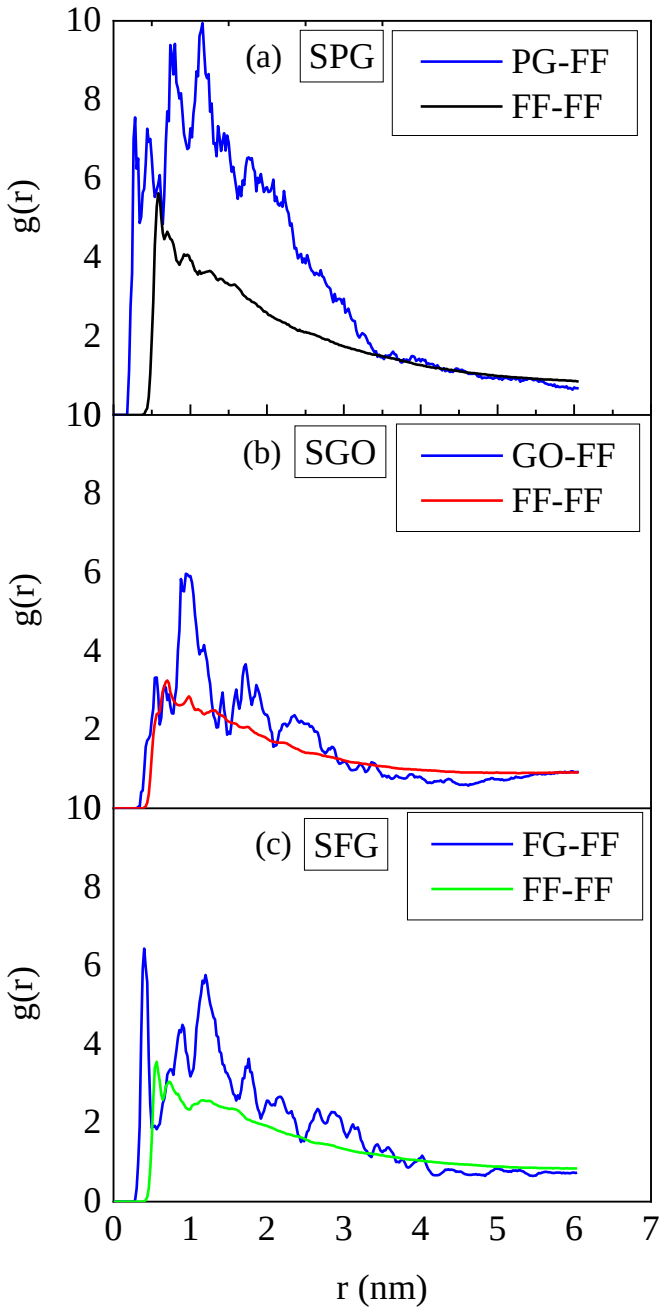

Figure 2. Comparison of RDFs (**a**) between FF-FF center of mass and PG atoms-FF center of mass, (**b**) between FF-FF center of mass and GO atoms-FF center of mass and (**c**) between FF-FF center of mass and FG atoms-FF center of mass.

Table 1. Average values of the radius of gyration (R_g) and the end-to-end distance (d) of the backbone of FF molecules, for SPG, SGO, and SFG systems.

	SPG	**SGO**	**SFG**
d (nm)	0.577 ± 0.002	0.573 ± 0.002	0.578 ± 0.002
R_g (nm)	0.387 ± 0.001	0.386 ± 0.001	0.388 ± 0.001

Based on the above measures, a rough estimation of the number of dipeptides (x) needed to cover a sheet of area A = 5 × 5 nm^2, on both sides, provides a value of 107 (i.e., $\left(x = 2\frac{A}{2R_g d}\right)$ where R_g = 0.390 nm is the radius of gyration of a FF in bulk and

d = 0.599 nm is the end-to-end distance of the backbone of FF), which is the same for all three nanosheets. Thus, there is an excess of ~(600 − 4 × 107 = 172) dipeptides in the systems, which can self-assemble to achieve a preferred structure.

Characteristic snapshots are shown in Figure 3b–d for SPG, SGO, and SFG, respectively. An obvious aggregation of dipeptides on the surfaces is shown in all cases, with the remaining dipeptides forming self-assembled structures on top of them. Figure 3a portrays an initial configuration for SPG system, where all FF molecules and graphene nanosheets are uniformly distributed in the aqueous phase. Similar are the initial configurations for the other two systems. Note here that for clarity, the water molecules are omitted from all snapshots.

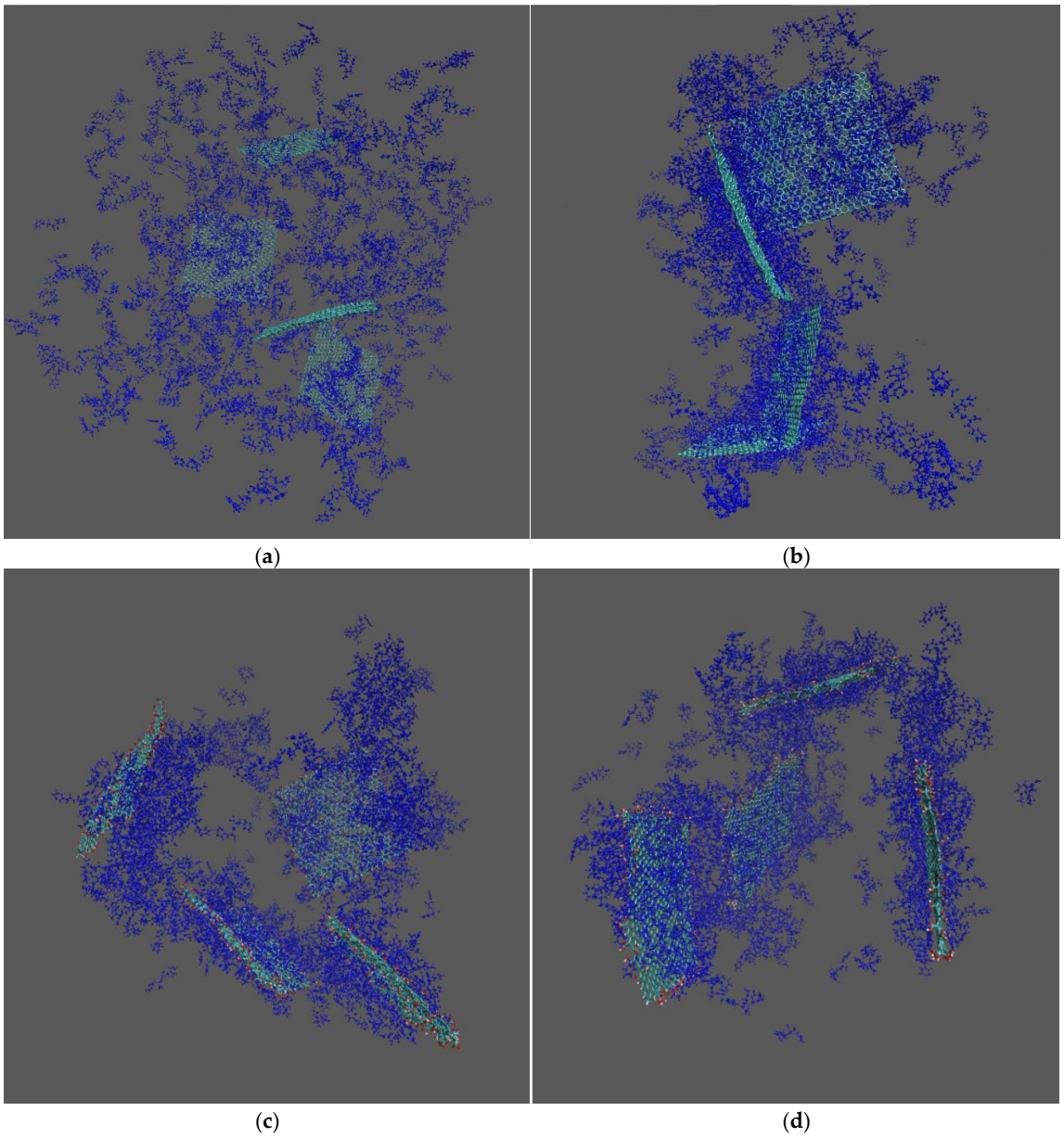

Figure 3. Characteristic snapshots of the initial configuration of SPG (**a**) and the equilibrated configurations of SPG (**b**), SGO (**c**), and SFG (**d**).

An additional comparison among the three nanocomposites, concerning the distribution of dipeptides with respect to the nanoflakes, is given by the calculation of the probability distribution of the distances between the atoms of FF and the atoms of the

nanosheets, which is presented in Figure 4. Calculations have been performed over the equilibrated part of the trajectory. At short distances, up to ~3 nm distributions are similar for all three systems. Then, compared to SGO and SFG, which exhibit similar distributions, with a peak around 6 nm, the SPG system displays distinct characteristics. More specifically, the SPG curve shows lower values between 3 nm and 10 nm and extends further at longer distances. Additionally, the peak for the SPG system is shifted towards longer distances, appearing around 9 nm. This observation suggests that upon interfacial layer formation, FF dipeptides do not increase layer thickness, but instead initiate self-assembly on top of PG, extending out of the plane (Figure 3b), which is not the case for the systems with the functionalized nanosheets.

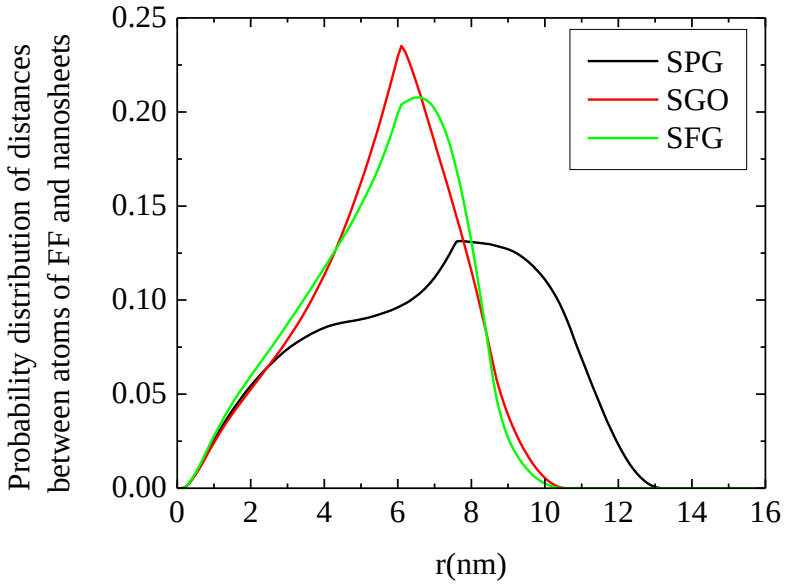

Figure 4. Probability distribution of the distance of FF atoms around nanosheet atoms for SPG, SGO, and SFG systems.

The arrangement of dipeptides with respect to the surfaces and to themselves, determines the wetting of graphene-based nanoflakes, as well as their own exposure to water. The solvent accessible surface area (SASA) of both FF and nanosheets per molecule as a function of time is presented in Figure 5a for FF and Figure 5b, 5c, and 5d for PG, FG, and GO, respectively. The interfacial layer of FF on PG is more exposed to water compared to that on FG and on GO, due to the homogeneity of PG flake, which favors a flatter dipeptide arrangement increasing the free space for water access. Additionally, the more extended, with respect to surface, self-assembled structure of FF on top of PG offers a larger area of dipeptides accessible to solvent molecules compared to that in SGO and SFG, where FF seem to form thick coating layers around the nanoflakes. Thus, in nanocomposites with the functionalized sheets, the SASA of FF is very similar.

The SASA of nanoflakes (Figure 5b–d) follows an increasing order PG < FG < GO, with the last two close to each other. A small decrease in SASA is observed with time for PG and FG, which is stabilized at around 40 ns, whereas the value is constant for GO. This is attributed to the gradual coverage of the nanosheets from FF, which modifies the available area for the solvent. However, in SGO, the functional groups on the GO surface keep the FF molecules further apart than on the other two flakes, maintaining almost the same free space for water molecules even after the completion of the coating. The average values of SASA over the last 20 ns of the trajectory (i.e., equilibrated part of the trajectory) are presented in Table 2.

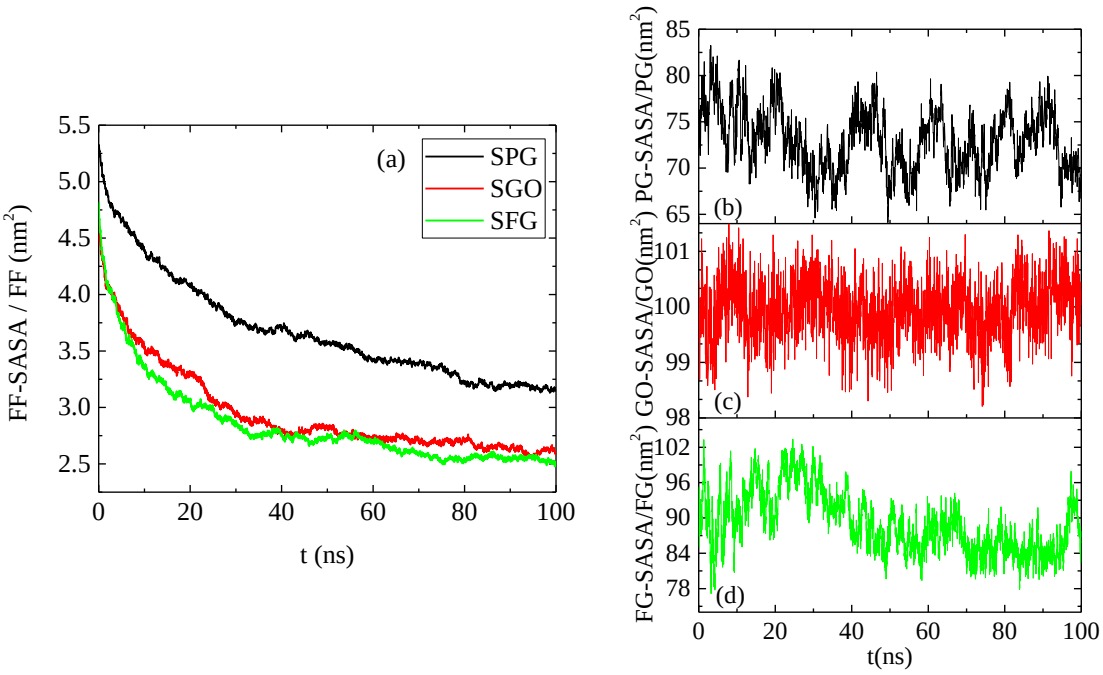

Figure 5. The solvent accessible surface area of (**a**) FF molecules per FF molecule in each system, (**b**) of PG, (**c**) of GO, and (**d**) of FG per nanosheet as a function of time.

Table 2. Average values of the solvent accessible surface area (SASA) of FF peptides per FF and of graphene nanosheets per nanosheet.

SASA (nm^2)	SPG	SGO	SFG
FF	3.191 ± 0.024	2.446 ± 0.029	2.547 ± 0.021
nanosheet	73.121 ± 2.996	99.905 ± 0.459	85.499 ± 3.151

2.2. Energetics

The energetic contributions to the assembly process are analyzed in the following, for all pair interactions between the different molecules in the systems. Table 3 includes average values for the Van der Waals and the electrostatic interactions over the equilibrated part of the trajectory for the three systems. As expected, enhanced electrostatic interactions are observed in the systems with the functionalized nanosheets, compared to the nanocomposite system with PG. The strongest attraction is met between FF and GO, almost half of it is that between FF and FG, whereas for FF-PG, it is much weaker. This is due to the charged functional groups, which are absent from PG, appear only around the edges in FG and all over the flake in GO. Similarly, electrostatic interactions between nanosheets are strongest in SGO, but the order reverses for SPG and SFG, with stronger attraction between PG flakes, coming from the partial charges of carbon atoms and possibly from their closer approximation. On the other hand, the electrostatic attraction between FF dipeptides is similar in all three nanocomposites, therefore this is not affected by the different nanofillers. As a consequence of the SASA (Table 2), nanosheet-water attraction has the lowest value for PG, FG follows and GO attains the highest value. FF-water Coulombic interactions are also strongest in SPG whereas, SFG and FGO have similar values, in agreement with their corresponding SASA. In all cases, the FF-FF electrostatic attraction dominates in comparison to the FF-nanosheet.

Table 3. Average values of the Lennard Jones and Coulomb interactions between FF-FF, FF-nanosheets, FF-water, nanosheet-nanosheet, and nanosheet-water molecules, calculated over the equilibrated part of each system's trajectory.

Energy (kJ/mol)	SPG	SGO	SFG
Coulomb (FF-FF)	−625,472.82 ± 883.42	−624,726.43 ± 1520.14	−642,118.48 ± 7.23
Coulomb (FF-nanosheet)	−464.06 ± 52.46	−24,688.66 ± 1134.26	−11,218.56 ± 962.41
Coulomb (FF-Water)	−302,032.66 ± 1889.66	−251,514.51 ± 4254.17	−241,920.87 ± 2162.55
Coulomb (nanosheet-nanosheet)	−8556.72 ± 14.13	−34,489.96 ± 114.83	−5593.73 ± 37.19
Coulomb (nanosheet-Water)	−2364.74 ± 109.90	−10,262.29 ± 1949.36	−4947.82 ± 244.69
L-J (FF-FF)	−27,684.42 ± 222.96	−31,415.91 ± 602.40	−30,318.18 ± 243.81
L-J (FF-nanosheet)	−15,623.13 ± 133.15	−19,547.94 ± 276.86	−19,150.44 ± 196.88
L-J (FF-Water)	−5137.34 ± 492.37	−4929.80 ± 754.56	−5367.93 ± 422.77
L-J (nanosheet-nanosheet)	34,822.62± 118.66	−8838.69 ± 40.71	−5223.51 ± 92.93
L-J (nanosheet-Water)	−2601.64 ± 81.13	−464.31 ± 185.02	−1261.99 ± 104.92

Concerning the Van der Waals contribution, a considerable difference among the systems is observed in the interactions between nanosheets; where high attraction is found between GO, FG follows, whereas repulsion exists between PG flakes. Lennard Jones (LJ) attractive interactions between FF dipeptides and between FF and nanosheets are similar in the SGO and SFG systems but lower in SPG. Similar values are also attained for LJ attractions between FF and water molecules, while big differences observed in nanosheet-water interactions. The strongest attraction is found between water and PG, almost half of it is the water—FG attraction and much weaker is the water—GO attraction.

Overall, Coulombic interactions between FF and nanosheets dominate in the SGO and SFG systems whereas, in SPG, attraction originates mainly from Van der Waals interactions. In all systems, the self-assembly of FF is controlled by electrostatic attractions while, between nanoflakes, energetic contributions are different in each system. In SGO, Coulomb is the major contributor, in SFG, Coulomb and LJ are equivalent, while in SPG, although there is a weak Coulombic attraction, attributed to the partial charges of the carbon atoms, the LJ repulsion is much stronger.

All energy values between each system's components, listed in Table 3, signify the driving forces that govern the assembly process. An additional factor that determines the assembly is the formation of hydrogen bonds (HB). Hydrogen bonds are formed between FF dipeptides and between dipeptides and only the functionalized nanoflakes (i.e., GO and FG). The definition of HBs is based on geometric criteria between donors and acceptors as follows: $r \leq r_{HB} = 0.35$ nm and $\alpha \leq \alpha_{HB} = 30^{\circ}$, where r_{HB} corresponds to the first minimum of the RDF of the SPC water model [62], r is the distance between the donor and the acceptor, and α is the hydrogen–donor–acceptor angle. The number of HBs between all the components of the systems is presented in Table 4. A larger number of HBs between FF dipeptides per dipeptide is observed in the nanocomposites with functionalized flakes compared to those in the SPG system. This is a noticeable observation because of the opposite trend observed in the RDF curves between FF, in the three systems. Although the higher probability of finding one molecule close to the other, indicated by the higher peak of RDF in SPG (Figure 1a), the arrangement of FF molecules, especially those that do not participate to the coating, may be the reason for the reduced hydrogen bonding. The larger amount of FF molecules, which are extended out of the PG surface (see Figure 4), imposes a head-to-tail arrangement [52,63], which favors hydrogen bonding between the end groups, but loose hydrogen bonds between backbone available sites.

Table 4. The average number of hydrogen bonds formed between FF dipeptides per dipeptide (FF-FF/FF), between FF dipeptides and the nanosheets of each system per FF dipeptide (FF-nanosheet/FF), between FF dipeptides and water molecules per FF dipeptide (FF-W/FF), and between the nanosheets of each system and water molecules per nanosheet (nanosheet-W/nanosheet).

HBs	SPG	SGO	SFG
FF-FF/FF	0.733 ± 0.024	0.923 ± 0.032	1.048 ± 0.027
FF-nanosheet/FF	-	0.372 ± 0.024	0.281 ± 0.009
FF-W/FF	8.1215 ± 0.054	7.257 ± 0.094	7.082 ± 0.066
Nanosheet-W/nanosheet	-	208.865 ± 7.746	55.419 ± 2.272

Due to the existence of functional groups all over the GO surface, more HBs between GO nanosheets and FF per FF are formed, compared to those formed between FG and FF per FF. The same stands for nanosheet-water per nanosheet hydrogen bonding. A more detailed quantification of the role of the various types of functional groups of GO in the binding with FF is presented in Table 5, where the hydrogen bonds between each functional group and FF were calculated separately. Substantial hydrogen bond superiority is observed between FF molecules and COO^- functional groups, almost half of these are the hydrogen bonds between FF and hydroxyl groups, whereas epoxy groups have a minor contribution in hydrogen bonding. This observation is in agreement with reference [24] where it was found that FF molecules preferentially concentrate at the edges of the GO nanosheets, which have fewer oxygen-containing groups, stressing out the predominance of COOH hydrogen bonding. The HBs of FF with water per FF are more in SPG compared to the two other nanocomposites, in accordance with the SASA results.

Table 5. Average number of hydrogen bonds formed between FF dipeptides and the three types of functional groups of GO nanosheets per dipeptide.

HBs	SGO
FF-COO^-/FF	0.349 ± 0.022
FF-OH/FF	0.017 ± 0.004
FF-epoxy/FF	0.007 ± 0.003

HBs as a function of time are presented in Figure 6a for SPG and SFG and in 6b for SGO, providing a comparison between FF-FF and FF-nanosheet values and, thus, quantifying the kinetics of the whole assembly process. HBs between dipeptides increase with time as the self-assembly evolves and attain a plateau at times >80 ns. On the other hand, HBs between FF and nanosheets are stabilized at around ~50 ns for SFG whereas, in SGO, there is a slow increase which tends to a constant value at ~100 ns. The slower rate in the SGO is due to a continuous rearrangement of dipeptides on the GO surface after the completion of the interfacial layer, which is attributed to the functional groups that do not allow for a very stable surface coating.

Combining these results with the time evolution of SASA (Figure 5), we can conclude that the kinetics of nanostructure formation exhibit an initial, rapid phase of surface coating, subsequently followed by a process of dipeptide self-assembly. Thus, for SPG, coating is finished at ~40 ns (Figure 5b), whereas the self-assembly of FF continues beyond 80 ns (Figure 6a). For SFG, coating is completed at ~50 ns (Figures 5c and 6a) but the self-assembly of FF continues for another ~20 ns (Figure 6a). Finally, for SGO, FF dipeptides do not form a very stable interfacial layer; therefore, there is a simultaneous evolution of coating and self-assembly which seems to be stabilized at ~100 ns (Figure 6b).

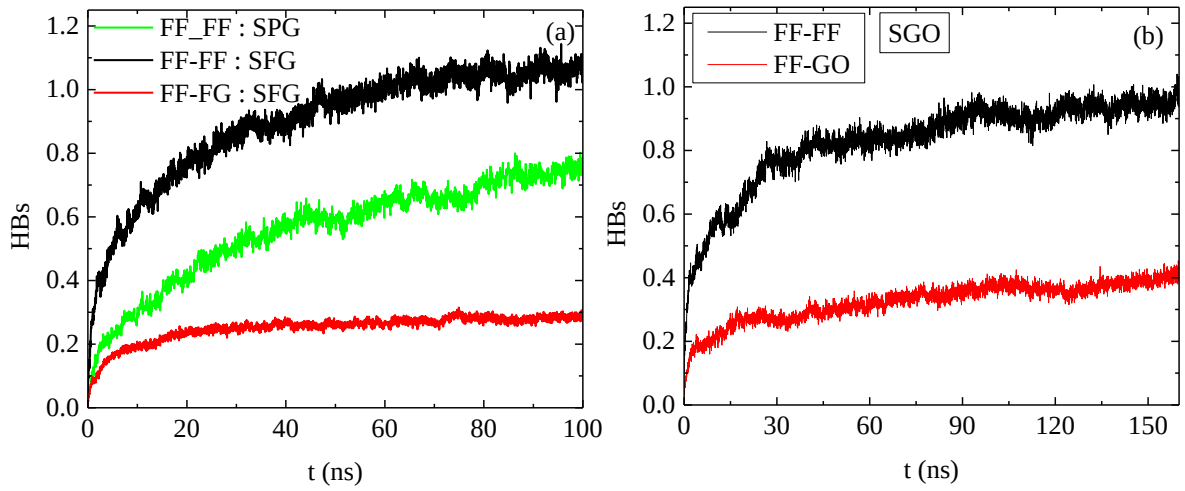

Figure 6. Average number of hydrogen bonds formed as a function of time (**a**) between FF dipeptides for SPG and between FF-FF and FF-FG for SFG; (**b**) between FF-FF and FF-GO for SGO.

2.3. Dynamics

Different nanofillers impact dipeptide dynamics in a different way as well. The effect becomes apparent and can be observed after assembly is finished. Therefore, the mean square displacement (MSD) of the center of mass of FF as a function of time is calculated over the last 20 ns of the trajectory and presented in Figure 7a. Considerably faster motion of FF is observed in SPG nanocomposite, compared to the systems with functionalized nanosheets, as a result of the reduced electrostatic interactions with the nanosheets in the former. However, similar are the MSDs in SFG and SGO, with the latter slightly slower. Despite the stronger interaction of FF with the GO nanosheet than with FG, the functional groups on the plane hinder close proximity. Thus, the entropic gain counterbalances the energetic excess, resulting in similar dynamical behavior of FF in SFG and SGO. The corresponding diffusion coefficients of FF in the nanocomposites are the following: $D_{(SPG)} = (0.1269 \pm 0.0167) \times 10^{-5}$ cm^2/s; $D_{(SFG)} = (0.0645 \pm 0.0095) \times 10^{-5}$ cm^2/s; and $D_{(SGO)} = (0.0385 \pm 0.0076) \times 10^{-5}$ cm^2/s.

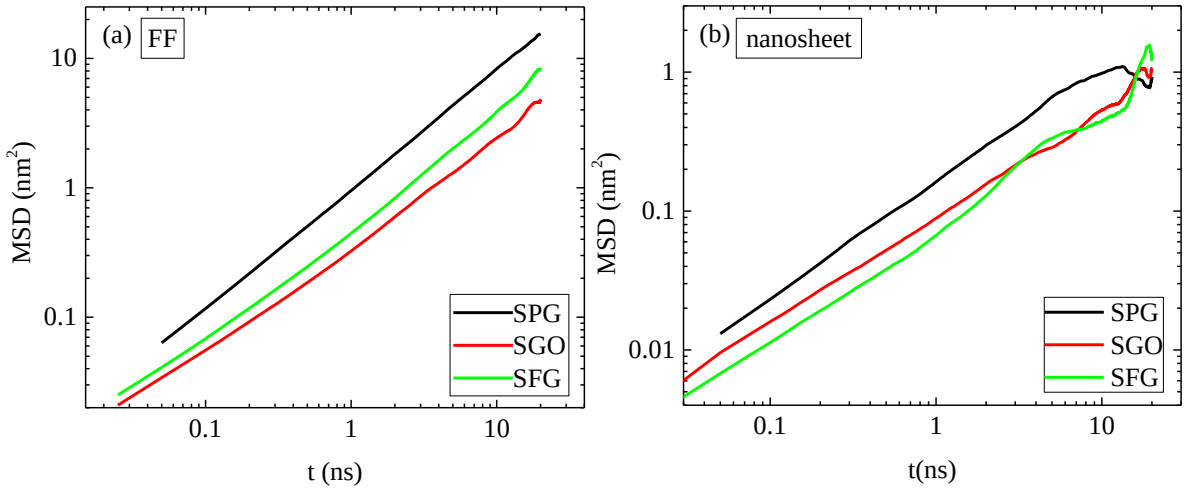

Figure 7. The mean square displacement of (**a**) the center of mass of FF dipeptides in SPG, SGO, and SFG systems and (**b**) the center of mass of the nanoflakes in SPG, SGO, and SFG systems, calculated over the last 20 ns of the simulations.

Similarly, the motion of the graphene-based nanosheets is affected by the FF dipeptides. It is interesting to observe how dipeptides impede the motion of the nanosheets effectively, preventing their stacking, particularly for PG, which exhibits a higher propensity for stacking due to the lack of functional groups. The MSD of the center of mass of the nanoflakes as a function of time is presented in Figure 7b for the last 20 ns of the trajectory, where the surface coating with FF has been completed. The corresponding diffusion coefficients of the nanoflakes in the nanocomposites are the following: $D_{PG} = (0.0330 \pm 0.0065) \times 10^{-5}$ cm^2/s; $D_{FG} = (0.0078 \pm 0.0065) \times 10^{-5}$ cm^2/s; and $D_{GO} = (0.0077 \pm 0.0062) \times 10^{-5}$ cm^2/s. Clearly, PG exhibits greater mobility compared to the functionalized nanosheets, which display comparable dynamic behavior. Furthermore, the MSD of the nanoflakes is approximately one order of magnitude lower than that of the dipeptides.

3. Systems and Simulation Method

Table 6 contains simulation details concerning the number of atoms of each nanographene sheet (N_g), the number of water molecules (N_s), the total number (N) of atoms in the system, the concentration (c), as well as the dimensions of the simulation box (L). Each system contains 600 FF dipeptides in their zwitterionic form and 4 graphene-based nanoflakes.

Table 6. Setup details for the simulated systems: the number of graphene atoms (N_g), the number of water molecules (N_s), the total number of atoms in the system (N), the concentration (c), and the dimensions of the simulation box (L).

System	N_g	N_s	N	$c(\mathbf{g\ cm^{-3}})$	$L(\mathbf{nm^3})$
SPG	4128	110,542	361,554	0.119	15.5 × 15.5 × 15.5
SGO	5136	51,953	186,967	0.2004	12.5 × 12.5 × 12.5
SFG	5208	51,047	184,149	0.204	12.4 × 12.4 × 12.4

The first system (SPG) consists of 600 dipeptides initially uniformly distributed in water and 4 identical rectangular pristine graphene (PG) nanosheets of dimensions 5 × 5 nm^2. PG nanosheets were modeled through an all-atom model used for graphite [64], where the molecule's Lennard Jones parameters were calculated using molecular mechanics simulations by Bellido et al. [65]. The second system (SGO) consists of four identical rectangular sheets of graphene oxide (GO) of dimensions 5 × 5 nm^2, 600 dipeptides, as well as 43 Na^+ in order to keep the solution electrically neutral, all initially uniformly distributed in water. The GO sheet was constructed using the software MakeGraphitics [66] which allows for the desired functionalization. Hydroxyl and epoxy groups were randomly distributed on both sides of the basal graphene plane, whereas ionized carboxyl groups were positioned at the edges of the sheet. More specifically, one ionized carboxyl group was placed every 2 peripheral carbons, resulting in a net charge for each GO sheet of $-43\,|e|$. The ratio of the hydroxyl to epoxy groups was 3:2, and the overall carbon to oxygen ratio was approximately kept to 5:1. Energetic parameters which describe bonded and non-bonded interactions were derived from the GAFF forcefield [67]. GAFF has been previously used and showed good performance in the calculation of the adsorption of small molecules on graphene oxide [31]. Finally, the third system (SFG) consists of 600 dipeptides initially uniformly distributed in water and 4 identical rectangular edge-functionalized graphene (FG) nanosheets of dimensions 5 × 5 nm^2. For the edge-functionalized graphene, a force field previously used for various carbon structures, which has been developed through ab initio calculations, has been chosen [68,69]. The FG sheet was designed to incorporate the appropriate number of carboxyl groups so the oxygen percentage is in accordance with

the experimental value of 12.68 wt% [70]. FG's functional groups were described via the OPLS-AA force field [71] and partial charges were assigned to all edge atoms. In all cases, for the dipeptide/graphene interactions, the Lorentz–Berthelot mixing rules (LB) were used [72]. The intermolecular and the intramolecular interactions for diphenylalanine were described with the AmberGS force field [73] in conjunction with the TIP3P water model [74] for the description of the solvent.

Atomistic molecular dynamics simulations utilizing the GROMACS simulation package [75,76] were performed for the study of the aforementioned systems. All systems were simulated in cubic simulation boxes, and periodic boundary conditions were applied in all three dimensions. After the proper preparation of the systems, energy minimization was performed using the steepest descend integrator to ensure that there were no steric clashes or inappropriate geometries in the system. Subsequently, production runs of [100–150] ns were conducted, and the equations of motion were integrated every 1 fs with the molecular dynamics leap-frog integrator. The hydrogen bonds were constrained using the LINCS algorithm [77]. Long-range electrostatic interactions were computed employing the PME method, with a cut-off radius of 1.0 nm. The systems were simulated in the isothermal-isobaric statistical ensemble, utilizing the velocity rescale algorithm to adjust the temperature to 300 K every 0.1 ps and the Berendsen algorithm to rescale the pressure to 1 atm every 0.5 ps.

4. Conclusions

This study focuses on a comprehensive investigation of the influence of various graphene-based nanosheets (pristine graphene (PG), graphene oxide (GO), and edge-functionalized graphene (FG)) on the self-assembly of FF dipeptides in water and the formed nanostructures. Utilizing all-atom molecular dynamics (MD) simulations, we initially examine how these different nanosheets impact the self-assembly mechanism of FF dipeptides in an aqueous solution under ambient conditions. Starting with a conformational analysis, a higher affinity of dipeptides with the surface, compared to themselves, is indicated by the corresponding RDF functions, resulting in the coating of nanosheets with FF, for all three systems, as an initial process. An interfacial layer rapidly forms on the graphene nanoflakes, consistent with experimental findings [59]. The coating layer is more stable in PG, whereas it can undergo rearrangements in the functionalized nanosheets, particularly in GO, where the presence of functional groups disrupts π-π* stacking between the dipeptide phenyl rings and the graphene plane, preventing the formation of a highly stable surface layer. The type of the nanofiller determines the self-assembled structure of the remaining FF molecules. In SGO and SFG, FF are placed on top of the interfacial layer, increasing its thickness, while in SPG, the remaining FF form a structure which extends at longer distances from the surface. FF-FF self-assembly, however, demonstrates a more dynamic equilibrium, gradually settling into a stable structure. The final nanostructures dictate the water exposure of both nanoflakes and dipeptides. SASA values for FF are highest in the SPG system compared to the other two, whereas the nanosheet's SASA is lowest for PG, followed by FG, with GO exhibiting the highest SASA, likely due to the higher density of functional groups, which increase the surface area of the flake.

The driving forces controlling the aforementioned nanostructures are dominated by Coulombic interactions between FF and nanosheets in the SGO and SFG systems while, in the SPG system, Van der Waals interactions determine the formed nanostructures. In the nanocomposites with the functionalized nanofillers, hydrogen bonds between FF and nanoflakes contribute also to the formation of the coating layer, mostly in the SGO system. Moreover, the self-assembly of FF is dominated by electrostatic attractions and hydrogen bonding between dipeptides.

The kinetics of nanostructure formation has an initial rapid process of surface coating, which is followed by further dipeptide self-assembly. In addition, there is a reciprocal effect on the dynamics of FF affected by the nanofillers and on the dynamics of the nanofillers affected by FF. Higher mobilities are found in SPG system for both FF and PG, though small differences are observed between SGO and SFG either for the dipeptides or for the nanoflakes. Although energy components and hydrogen bonds impose stronger interactions in SGO, the functional groups on the plane of GO prevent close proximity, so the entropic gain compensates for the excess energy, leading to comparable dynamics in the two systems with the functionalized nanoflakes.

The detailed information presented in the current study provides guidelines for the proper coordination of the interactions (i.e., the fraction, the type, and the position of functional groups) and the relative concentration of FF with respect to that of nanoflakes, in the nanocomposites, according to a desired application. The study of environmental effects, such as temperature, humidity, or pH could comprise future research directions to investigate their effect on the adsorption behavior of diphenylalanine on graphene-based materials. Understanding these effects could be vital for practical applications in varying conditions. The exploration of different FF-to-graphene ratios is also an interesting aspect which can help to identify the ideal balance for specific applications in order to optimize the properties of the nanocomposites. Using different dipeptide compositions, the thickness of the coating layer can also be determined on the different types of graphene-based nanosheets, as well as the structure of the remaining self-assembled dipeptides. Finally, further research could involve investigating the adsorption properties of other peptides on graphene, which could help in understanding the general behavior of peptide-graphene interactions and their implications for various applications in biomedicine and nanotechnology.

Author Contributions: Conceptualization: A.N.R.; methodology: A.N.R.; data analysis: E.M., G.S. and P.N.; validation of results: A.N.R.; writing—original draft preparation: A.N.R. and E.M.; supervising: A.N.R. All authors have read and agreed to the published version of the manuscript.

Funding: This research received no external funding.

Institutional Review Board Statement: Not applicable.

Informed Consent Statement: Not applicable.

Data Availability Statement: The original contributions presented in this study are included in the article. Further inquiries can be directed to the corresponding author.

Acknowledgments: The authors would like to thank the support of this work by computational time granted from Greek Research & Technology Network (GRNET) in the National HPC facility-ARIS for the Project: Peptide-Graphene nanocomposites though Molecular Simulations, BIOGRAPH.

Conflicts of Interest: The authors declare no conflicts of interest.

References

1. Ishraq, S.; Liu, Y. Synthesis, Characterization and Bioapplications of Pristine Graphene: A Review. *Univers. J. Carbon Res.* **2023**, *1*, 1–21. [CrossRef]
2. Zhao, S.; Zhao, Z.; Yang, Z.; Ke, L.L.; Kitipornchai, S.; Yang, J. Functionally Graded Graphene Reinforced Composite Structures: A Review. *Eng. Struct.* **2020**, *210*, 110339. [CrossRef]
3. Dasari, B.L.; Nouri, J.M.; Brabazon, D.; Naher, S. Graphene and Derivatives—Synthesis Techniques, Properties and Their Energy Applications. *Energy* **2017**, *140*, 766–778. [CrossRef]
4. Sang, M.; Shin, J.; Kim, K.; Yu, K.J. Electronic and Thermal Properties of Graphene and Recent Advances in Graphene Based Electronics Applications. *Nanomaterials* **2019**, *9*, 374. [CrossRef]
5. Liang, M.; Luo, B.; Zhi, L. Application of Graphene and Graphene-Based Materials in Clean Energy-Related Devices. *Int. J. Energy Res.* **2009**, *33*, 1161–1170. [CrossRef]

6. Shtein, M.; Nadiv, R.; Buzaglo, M.; Regev, O. Graphene-Based Hybrid Composites for Efficient Thermal Management of Electronic Devices. *ACS Appl. Mater. Interfaces* **2015**, *7*, 23725–23730. [CrossRef]
7. Das, T.; Sharma, B.K.; Katiyar, A.K.; Ahn, J.-H. Graphene-Based Flexible and Wearable Electronics. *J. Semicond.* **2018**, *39*, 11007. [CrossRef]
8. Burdanova, M.G.; Kharlamova, M.V.; Kramberger, C.; Nikitin, M.P. Applications of Pristine and Functionalized Carbon Nanotubes, Graphene, and Graphene Nanoribbons in Biomedicine. *Nanomaterials* **2021**, *11*, 3020. [CrossRef]
9. Han, S.; Sun, J.; He, S.; Tang, M.; Chai, R. The Application of Graphene-Based Biomaterials in Biomedicine. *Am. J. Transl. Res.* **2019**, *11*, 3246.
10. Zhang, H.; Grüner, G.; Zhao, Y. Recent Advancements of Graphene in Biomedicine. *J. Mater. Chem. B* **2013**, *1*, 2542–2567. [CrossRef]
11. Ferreras, A.; Matesanz, A.; Mendizabal, J.; Artola, K.; Nisina, Y.; Acedo, P.; Jorcano, J.; Ruiz Estrada, A.; Reina, G.; Martín Jiménez, C. Light-Responsive and Antibacterial Graphenic Materials as a Holistic Approach to Tissue Engineering. *ACS Nanosci. Au* **2024**, *4*, 263–272. [CrossRef] [PubMed]
12. Li, D.; Zhang, W.; Yu, X.; Wang, Z.; Su, Z.; Wei, G. When Biomolecules Meet Graphene: From Molecular Level Interactions to Material Design and Applications. *Nanoscale* **2016**, *8*, 19491–19509. [CrossRef] [PubMed]
13. Ji, G.; Tian, J.; Xing, F.; Feng, Y. Optical Biosensor Based on Graphene and Its Derivatives for Detecting Biomolecules. *Int. J. Mol. Sci.* **2022**, *23*, 838. [CrossRef] [PubMed]
14. Yin, S.; Yang, H.; Wu, Y.; Wang, Z.; Yu, C.; Tang, Y.; Wang, G. Recent Advances in Biological Molecule Detection Based on a Three-Dimensional Graphene Structure. *Analyst* **2024**, *149*, 1364–1380. [CrossRef]
15. Ye, J.; Fan, M.; Zhan, J.; Zhang, X.; Lu, S.; Chai, M.; Zhang, Y.; Zhao, X.; Li, S.; Zhang, D. In Silico Bioactivity Prediction of Proteins Interacting with Graphene-Based Nanomaterials Guides Rational Design of Biosensor. *Talanta* **2024**, *277*, 126397. [CrossRef]
16. Kakatkar, A.; Abhilash, T.; De Alba, R.; Parpia, J.; Craighead, H. Detection of DNA and Poly-l-Lysine Using CVD Graphene-Channel FET Biosensors. *Nanotechnology* **2015**, *26*, 125502. [CrossRef]
17. Texter, J. Graphene Dispersions. *Curr. Opin. Colloid. Interface Sci.* **2014**, *19*, 163–174. [CrossRef]
18. Su, R.; Zhang, X. Wettability and Surface Free Energy Analyses of Monolayer Graphene. *J. Therm. Sci.* **2018**, *27*, 359–363. [CrossRef]
19. Bourdo, S.E.; Al Faouri, R.; Sleezer, R.; Nima, Z.A.; Lafont, A.; Chhetri, B.P.; Benamara, M.; Martin, B.; Salamo, G.J.; Biris, A.S. Physicochemical Characteristics of Pristine and Functionalized Graphene. *J. Appl. Toxicol.* **2017**, *37*, 1288–1296. [CrossRef]
20. Zhang, Y.; Wu, C.; Zhang, J. Interactions of Graphene and Graphene Oxide with Proteins and Peptides. *Nanotechnol. Rev.* **2013**, *2*, 27–45. [CrossRef]
21. Margani, F.; Magrograssi, M.; Piccini, M.; Brambilla, L.; Galimberti, M.; Barbera, V. Facile Edge Functionalization of Graphene Layers with a Biosourced 2-Pyrone. *ACS Sustain. Chem. Eng.* **2022**, *10*, 4082–4093. [CrossRef]
22. Bačová, P.; Rissanou, A.N.; Harmandaris, V. Edge-Functionalized Graphene as a Nanofiller: Molecular Dynamics Simulation Study. *Macromolecules* **2015**, *48*, 9024–9038. [CrossRef]
23. Mathesh, M.; Liu, J.; Nam, N.D.; Lam, S.K.H.; Zheng, R.; Barrow, C.J.; Yang, W. Facile Synthesis of Graphene Oxide Hybrids Bridged by Copper Ions for Increased Conductivity. *J. Mater. Chem. C* **2013**, *1*, 3084–3090. [CrossRef]
24. Trapani, G.; Caruso, V.C.L.; Cucci, L.M.; Attanasio, F.; Tabbì, G.; Forte, G.; La Mendola, D.; Satriano, C. Graphene Oxide Nanosheets Tailored with Aromatic Dipeptide Nanoassemblies for a Tuneable Interaction with Cell Membranes. *Front. Bioeng. Biotechnol.* **2020**, *8*, 427. [CrossRef]
25. Baweja, L.; Balamurugan, K.; Subramanian, V.; Dhawan, A. Effect of Graphene Oxide on the Conformational Transitions of Amyloid Beta Peptide: A Molecular Dynamics Simulation Study. *J. Mol. Graph. Model.* **2015**, *61*, 175–185. [CrossRef]
26. Wang, Q.; Jiang, N.; Fu, B.; Huang, F.; Liu, J. Self-Assembling Peptide-Based Nanodrug Delivery Systems. *Biomater. Sci.* **2019**, *7*, 4888–4911. [CrossRef]
27. Yin, L.; Yuvienco, C.; Montclare, J.K. Protein Based Therapeutic Delivery Agents: Contemporary Developments and Challenges. *Biomaterials* **2017**, *134*, 91–116. [CrossRef]
28. Gao, Y.; Wang, L.; Zhang, X.; Zhou, Z.; Shen, X.; Hu, H.; Sun, R.; Tang, J. Advances in Self-Assembled Peptides as Drug Carriers. *Pharmaceutics* **2023**, *15*, 482. [CrossRef]
29. Naskar, J.; Roy, S.; Joardar, A.; Das, S.; Banerjee, A. Self-Assembling Dipeptide-Based Nontoxic Vesicles as Carriers for Drugs and Other Biologically Important Molecules. *Org. Biomol. Chem.* **2011**, *9*, 6610–6615. [CrossRef]
30. Lee, S.; Trinh, T.H.T.; Yoo, M.; Shin, J.; Lee, H.; Kim, J.; Hwang, E.; Lim, Y.B.; Ryou, C. Self-Assembling Peptides and Their Application in the Treatment of Diseases. *Int. J. Mol. Sci.* **2019**, *20*, 5850. [CrossRef]
31. Saeedimasine, M.; Brandt, E.G.; Lyubartsev, A.P. Atomistic Perspective on Biomolecular Adsorption on Functionalized Carbon Nanomaterials under Ambient Conditions. *J. Phys. Chem. B* **2021**, *125*, 416–430. [CrossRef] [PubMed]
32. De La Rica, R.; Matsui, H. Applications of Peptide and Protein-Based Materials in Bionanotechnology. *Chem. Soc. Rev.* **2010**, *39*, 3499–3509. [CrossRef] [PubMed]

33. Shao, X.; Yan, C.; Wang, C.; Wang, C.; Cao, Y.; Zhou, Y.; Guan, P.; Hu, X.; Zhu, W.; Ding, S. Advanced Nanomaterials for Modulating Alzheimer's Related Amyloid Aggregation. *Nanoscale Adv.* **2022**, *5*, 46–80. [CrossRef] [PubMed]
34. Kim, S.H.; Kaplan, J.A.; Sun, Y.; Shieh, A.; Sun, H.-L.; Croce, C.M.; Grinstaff, M.W.; Parquette, J.R. The Self-Assembly of Anticancer Camptothecin–Dipeptide Nanotubes: A Minimalistic and High Drug Loading Approach to Increased Efficacy. *Chem.-Eur. J.* **2015**, *21*, 101–105. [CrossRef]
35. Yang, Z.; Ge, C.; Liu, J.; Chong, Y.; Gu, Z.; Jimenez-Cruz, C.A.; Chai, Z.; Zhou, R. Destruction of Amyloid Fibrils by Graphene through Penetration and Extraction of Peptides. *Nanoscale* **2015**, *7*, 18725–18737. [CrossRef]
36. Li, C.; Adamcik, J.; Mezzenga, R. Biodegradable Nanocomposites of Amyloid Fibrils and Graphene with Shape-Memory and Enzyme-Sensing Properties. *Nat. Nanotechnol.* **2012**, *7*, 421–427. [CrossRef]
37. Xiuhua, Y.; Baoyu, L.; Liu, S.; Gu, Z.; Zhou, B.; Yang, Z. Effect of the Surface Curvature on Amyloid-β Peptide Adsorption for Graphene. *RSC Adv.* **2019**, *9*, 10094–10099. [CrossRef]
38. Mahmoudi, M.; Akhavan, O.; Ghavami, M.; Rezaee, F. Graphene Oxide Strongly Inhibits Amyloid Beta Fibrillation. *Nanoscale* **2012**, *4*, 7322–7325. [CrossRef]
39. Li, Q.; Liu, L.; Zhang, S.; Xu, M.; Wang, X.; Wang, C.; Besenbacher, F.; Dong, M. Modulating Aβ33–42 Peptide Assembly by Graphene Oxide. *Chem. Eur. J.* **2014**, *20*, 7236–7240. [CrossRef]
40. Jie, W.; Cao, Y.; Li, Q.; Liu, L.; Dong, M. Size Effect of Graphene Oxide on Modulating Amyloid Peptide Assembly. *Chem. Eur. J.* **2015**, *21*, 9632–9637. [CrossRef]
41. Chen, Y.; Chen, Z.; Sun, Y.; Lei, J.; Wei, G. Mechanistic Insights into the Inhibition and Size Effects of Graphene Oxide Nanosheets on the Aggregation of an Amyloid-β Peptide Fragment. *Nanoscale* **2018**, *10*, 8989–8997. [CrossRef] [PubMed]
42. Jin, Y.; Sun, Y.; Chen, Y.; Lei, J.; Wei, G. Molecular Dynamics Simulations Reveal the Mechanism of Graphene Oxide Nanosheet towards the Inhibition of Aβ1-42 Peptide Aggregation. *Phys. Chem. Chem. Phys.* **2019**, *21*, 10981–10991. [CrossRef] [PubMed]
43. He, H.; Xu, J.; Li, C.; Gao, T.; Jiang, P.; Jiang, F.-L.; Liu, Y. Insights into Mechanism of Aβ42 Fibril Growth on Surface of Graphene Oxides: Oxidative Degree Matters. *Adv. Health Mater.* **2021**, *10*, 2100436. [CrossRef] [PubMed]
44. No, Y.H.; Kim, N.H.; Gnapareddy, B.; Choi, B.; Kim, Y.T.; Dugasani, S.R.; Lee, O.S.; Kim, K.H.; Ko, Y.S.; Lee, S.; et al. Nature-Inspired Construction of Two-Dimensionally Self-Assembled Peptide on Pristine Graphene. *J. Phys. Chem. Lett.* **2017**, *8*, 3734–3739. [CrossRef]
45. Silva-Alves, D.A.; Camara, M.V.S.; Chaves-Neto, A.M.J.; Gester, R.; Andrade-Filho, T. Theoretical Study of the Adsorption of Diphenylalanine on Pristine Graphene. *Theor. Chem. Acc.* **2020**, *139*, 83. [CrossRef]
46. Camden, A.N.; Barr, S.A.; Berry, R.J. Simulations of Peptide-Graphene Interactions in Explicit Water. *J. Phys. Chem. B* **2013**, *117*, 10691–10697. [CrossRef]
47. Akdim, B.; Pachter, R.; Kim, S.S.; Naik, R.R.; Walsh, T.R.; Trohalaki, S.; Hong, G.; Kuang, Z.; Farmer, B.L. Electronic Properties of a Graphene Device with Peptide Adsorption: Insight from Simulation. *ACS Appl. Mater. Interfaces* **2013**, *5*, 7470–7477. [CrossRef]
48. Cheng, Y.; Koh, L.-D.; Li, D.; Ji, B.; Zhang, Y.; Yeo, J.; Guan, G.; Han, M.-Y.; Zhang, Y.-W. Peptide–Graphene Interactions Enhance the Mechanical Properties of Silk Fibroin. *ACS Appl. Mater. Interfaces* **2015**, *7*, 21787–21796. [CrossRef]
49. Huang, R.; Qi, W.; Su, R.; Zhao, J.; He, Z. Solvent and Surface Controlled Self-Assembly of Diphenylalanine Peptide: From Microtubes to Nanofibers. *Soft Matter* **2011**, *7*, 6418–6421. [CrossRef]
50. Yan, X.; Zhu, P.; Li, J. Self-Assembly and Application of Diphenylalanine-Based Nanostructures. *Chem. Soc. Rev.* **2010**, *39*, 1877–1890. [CrossRef]
51. Kim, J.; Han, T.H.; Kim, Y.I.; Park, J.S.; Choi, J.; Churchill, D.G.; Kim, S.O.; Ihee, H. Role of Water in Directing Diphenylalanine Assembly into Nanotubes and Nanowires. *Adv. Mater.* **2010**, *22*, 583–587. [CrossRef] [PubMed]
52. Tamamis, P.; Adler-Abramovich, L.; Reches, M.; Marshall, K.; Sikorski, P.; Serpell, L.; Gazit, E.; Archontis, G. Self-Assembly of Phenylalanine Oligopeptides: Insights from Experiments and Simulations. *Biophys. J.* **2009**, *96*, 5020–5029. [CrossRef] [PubMed]
53. Rissanou, A.N.; Georgilis, E.; Kasotakis, E.; Mitraki, A.; Harmandaris, V. Effect of Solvent on the Self-Assembly of Dialanine and Diphenylalanine Peptides. *J. Phys. Chem. B* **2013**, *117*, 3962–3975. [CrossRef] [PubMed]
54. Anderson, J.; Lake, P.T.; McCullagh, M. Initial Aggregation and Ordering Mechanism of Diphenylalanine from Microsecond All-Atom Molecular Dynamics Simulations. *J. Phys. Chem. B* **2018**, *122*, 12331–12341. [CrossRef]
55. da Silveira, G.D.; Izabelle, C.; Saubamea, B.; Varenne, A.; d'Orlyé, F. Insights into Diphenylalanine Peptide Self-Assembled Nanostructures for Integration as Nanoplatforms in Analytical and Medical Devices. *Int. J. Pharm.* **2023**, *648*, 123559. [CrossRef]
56. Jeon, J.; Mills, C.E.; Shell, M.S. Molecular Insights into Diphenylalanine Nanotube Assembly: All-Atom Simulations of Oligomerization. *J. Phys. Chem. B* **2013**, *117*, 3935–3943. [CrossRef]
57. Nguyen, V.; Zhu, R.; Jenkins, K.; Yang, R. Self-Assembly of Diphenylalanine Peptide with Controlled Polarization for Power Generation. *Nat. Commun.* **2016**, *7*, 13566. [CrossRef]
58. Ravikumar, A.; Natraj, V.; Verma, A.; Sivagnanam, S.; Sivalingam, Y.; Das, P.; Surya, V.J.; Han, W.H.; Liu, N. Wearable Sensors for Real-Time Physiological Monitoring Based on Self-Assembled Diphenylalanine Peptide Nanostructures. *Surf. Interfaces* **2023**, *39*, 102986. [CrossRef]

59. Bhattacharya, A.; Cheng, J.; Bhosale, S.; Aphale, A.; Macwan, I.; Patra, P.K.; Mukerji, I. UV Resonance Raman Characterization of Diphenylalanine-Graphene Nanotubes. *Spectroscopy* **2012**, *27*, 40.
60. Ryan, K.; Neumayer, S.M.; Maraka, H.V.R.; Buchete, N.V.; Kholkin, A.L.; Rice, J.H.; Rodriguez, B.J. Thermal and Aqueous Stability Improvement of Graphene Oxide Enhanced Diphenylalanine Nanocomposites. *Sci. Technol. Adv. Mater.* **2017**, *18*, 172–179. [CrossRef]
61. Rissanou, A.N.; Keliri, A.; Arnittali, M.; Harmandaris, V. Self-Assembly of Diphenylalanine Peptides on Graphene: Via Detailed Atomistic Simulations. *Phys. Chem. Chem. Phys.* **2020**, *22*, 27645–27657. [CrossRef] [PubMed]
62. van der Spoel, D.; van Maaren, P.J.; Larsson, P.; Tîmneanu, N. Thermodynamics of Hydrogen Bonding in Hydrophilic and Hydrophobic Media. *J. Phys. Chem. B* **2006**, *110*, 4393–4398. [CrossRef] [PubMed]
63. Tamamis, P.; Kasotakis, E.; Mitraki, A.; Archontis, G. Amyloid-like Self-Assembly of Peptide Sequences from the Adenovirus Fiber Shaft: Insights from Molecular Dynamics Simulations. *J. Phys. Chem. B* **2009**, *113*, 15639–15647. [CrossRef]
64. Steele, W.A. The Physical Interaction of Gases with Crystalline Solids: I. Gas-Solid Energies and Properties of Isolated Adsorbed Atoms. *Surf. Sci.* **1973**, *36*, 317–352. [CrossRef]
65. Bellido, E.P.; Seminario, J.M. Molecular Dynamics Simulations of Folding of Supported Graphene. *J. Phys. Chem. C* **2010**, *114*, 22472–22477. [CrossRef]
66. Sinclair, R.C. Make-Graphitics-Github. GitHub. Available online: https://github.com/velocirobbie/make-graphitics (accessed on 8 January 2025).
67. Wang, J.; Wolf, R.M.; Caldwell, J.W.; Kollman, P.A.; Case, D.A. Development and Testing of a General Amber Force Field. *J. Comput. Chem.* **2004**, *25*, 1157–1174. [CrossRef]
68. Walther, J.H.; Jaffe, R.; Halicioglu, T.; Koumoutsakos, P. Carbon Nanotubes in Water: Structural Characteristics and Energetics. *J. Phys. Chem. B* **2001**, *105*, 9980–9987. [CrossRef]
69. Pandey, Y.N.; Brayton, A.; Burkhart, C.; Papakonstantopoulos, G.J.; Doxastakis, M. Multiscale Modeling of Polyisoprene on Graphite. *J. Chem. Phys.* **2014**, *140*, 054908. [CrossRef]
70. Gao, W.; Alemany, L.B.; Ci, L.; Ajayan, P.M. New Insights into the Structure and Reduction of Graphite Oxide. *Nat. Chem.* **2009**, *1*, 403–408. [CrossRef] [PubMed]
71. Jorgensen, W.L.; Maxwell, D.S.; Tirado-Rives, J. Development and Testing of the OPLS All-Atom Force Field on Conformational Energetics and Properties of Organic Liquids. *J. Am. Chem. Soc.* **1996**, *118*, 11225–11236. [CrossRef]
72. Lorentz, H.A. Ueber Die Anwendung Des Satzes Vom Virial in Der Kinetischen Theorie Der Gase. *Ann. Phys.* **1881**, *248*, 127–136. [CrossRef]
73. García, A.E.; Sanbonmatsu, K.Y. Helical Stabilization by Side Chain Shielding of Backbone Hydrogen Bonds. *Proc. Natl. Acad. Sci. USA* **2002**, *99*, 2782–2787. [CrossRef] [PubMed]
74. Jorgensen, W.L.; Chandrasekhar, J.; Madura, J.D.; Impey, R.W.; Klein, M.L. Comparison of Simple Potential Functions for Simulating Liquid Water. *J. Chem. Phys.* **1983**, *79*, 926–935. [CrossRef]
75. Van Der Spoel, D.; Lindahl, E.; Hess, B.; Groenhof, G.; Mark, A.E.; Berendsen, H.J.C. GROMACS: Fast, Flexible, and Free. *J. Comput. Chem.* **2005**, *26*, 1701–1718. [CrossRef]
76. Berendsen, H.J.C.; van der Spoel, D.; van Drunen, R. GROMACS: A Message-Passing Parallel Molecular Dynamics Implementation. *Comput. Phys. Commun.* **1995**, *91*, 43–56. [CrossRef]
77. Hess, B.; Bekker, H.; Berendsen, H.J.C.; Fraaije, J.G.E.M. LINCS: A Linear Constraint Solver for Molecular Simulations. *J. Comput. Chem.* **1997**, *18*, 1463–1472. [CrossRef]

Disclaimer/Publisher's Note: The statements, opinions and data contained in all publications are solely those of the individual author(s) and contributor(s) and not of MDPI and/or the editor(s). MDPI and/or the editor(s) disclaim responsibility for any injury to people or property resulting from any ideas, methods, instructions or products referred to in the content.